Dynamics of particles trapping and detrapping in coherent wave packets

David L. Bruhwiler[1] and John R. Cary[2]
[1]Grumman Research and Development Center, 4 Independence Way, Princeton, New Jersey 08540-6620
[2]Department of Astrophysical, Planetary and Atmospheric Sciences and Department of Physics, University of Colorado, Boulder, Colorado 80309-0391
(Received 3 August 1994)

Particles interacting resonantly with large-amplitude coherent one-dimensional wave packets can trap and subsequently detrap or even reflect. Many resonant particles are strongly scattered in the process, and the long-time dynamics of such particles is stochastic throughout a large region of phase space when repeated wave-particle interactions occur. We apply adiabatic invariance theory and separatrix crossing theory to this Hamiltonian system, which is beyond the realm of quasilinear theory. We calculate the adiabatic invariant through first order in the (small) slowness parameter ε for all particle trajectories. Because the trajectories of resonant particles cross a separatrix, the adiabatic invariant is broken and separatrix-crossing theory must be used. Our Hamiltonian provides a simple model for the fundamental physics of narrow-spectrum plasma turbulence, for strong rf current drive in a tokamak, and for electron dynamics in a recirculating free-electron laser.

PACS number(s): 52.20.Dq, 52.25.Fi, 52.25.Tx, 52.35.Ra

I. INTRODUCTION

The resonant interaction of particles with electrostatic plasma waves has been a fundamental issue in plasma physics for decades, beginning with Landau damping [1] and quasilinear diffusion [2]. These early analyses involved small-field expansions, as well as the related assumption that the bounce time of trapped particles is long compared to other relevant time scales. Here we consider the opposite limit of arbitrarily large field amplitudes, and we directly address the issue of particle trajectories that trap in a wave packet and subsequently execute many bounce oscillations.

Quasilinear theory is appropriate for what is now known as weak plasma turbulence. Dupree [3] derived a simple criterion for the transition from weak turbulence to strong turbulence, based on two time scales. The first time scale, $\tau_b \sim (m/ek^2V_0)^{1/2}$, is the bounce time of a particle with charge e and mass m, deeply trapped in a sinusoidal electrostatic potential of wave number k and maximum amplitude V_0. The second time scale, $\tau_{\text{auto}} \sim 1/k\Delta v_\phi$, is the field autocorrelation time, where k is the central wave number of a given wave spectrum, and Δv_ϕ is the characteristic separation between maximum and minimum phase velocities.

In the weak turbulence limit $\tau_{\text{auto}} \ll \tau_b$, the waves rearrange themselves before a particle can execute a bounce oscillation under the influence of a single wave; therefore, the particle is kicked randomly from wave to wave. This limit occurs when the electric fields are small and the spectrum of phase velocities is broad. The strong turbulence limit $\tau_b \ll \tau_{\text{auto}}$, is characterized by a narrow spectrum of large electric fields, so a particle can execute many bounce oscillations before the relative wave phases have changed significantly. This is the dynamical regime treated here.

Quasilinear theory was originally developed in a self-consistent context by using perturbation theory to solve the Vlasov and Poisson equations; however, Doveil and Grésillon [4] showed that it could very naturally be applied to test particles interacting with a random spectrum of applied electrostatic fields. They calculated a quasilinear diffusion coefficient which compared well with numerical simulations for $\tau_{\text{auto}}/\tau_b < 0.4$. Fuchs, Krapchev, Ram, and Bers [5] (whom we will refer to henceforth as FKRB) took quasilinear theory one step further from its original context by applying it to test particles interacting with a coherent one-dimensional (1D) wave packet having a Gaussian envelope. They also calculated a quasilinear diffusion coefficient, obtaining good agreement between theory and numerics for $\tau_{\text{auto}}/\tau_b < 0.2$, where for their system the autocorrelation time is simply the transit time of a resonant particle moving through the wave packet.

The numerical work of FKRB showed that, in the limit $\tau_{\text{auto}} > \tau_b$, the particle dynamics was dominated by strong scattering (with even reflections occurring for large enough amplitudes), not by small, diffusive changes in the velocity. Qualitatively the same result was found numerically by Graham and Fejer [6] for particle dynamics in a random field of waves with a narrow spectrum of phase velocities. Thus the dynamics of test particles interacting with a localized, large-amplitude coherent wave packet is similar to the dynamics of test particles in a narrow spectrum of random, large-amplitude electric fields.

We have chosen to explore the dynamics of wave-particle interactions in the strong turbulence limit by considering a coherent wave packet very similar to the model studied in FKRB. Our model becomes equivalent to that of FKRB in the limit that the wave packet is very broad, which is the limit of interest here. Two important dimensionless parameters which arise in our analysis are the slowness parameter ε and the maximum wave ampli-

1063-651X/94/50(5)/3949(13)/$06.00

tude α_0. The slowness parameter $\varepsilon \sim 1/kL \ll 1$, where L is the characteristic length scale of the wave envelope, is inversely proportional to the number of spatial wave oscillations within the envelope of the wave packet. The amplitude $\alpha_0 = (k^2 e/m\omega^2)V_0$, where ω is the wave frequency, is the maximum wave amplitude in our dimensionless units, and is assumed here to be of order unity.

The Hamiltonian system we treat here contains the two distinct time scales discussed above. The slowness parameter $\varepsilon \ll 1$ controls the slow time scale over which wave parameters vary (essentially, the transit time τ_{auto}). In fact, by Fourier transforming our wave model to obtain the spectrum of wave numbers, one can show in the limit $\varepsilon \ll 1$ that $\tau_{\text{auto}} \sim 1/(\varepsilon\omega)$. The rapid oscillations of particle phase with respect to the wave occur on the fast time scale, the bounce time in the region of maximum wave amplitude, $\tau_b \sim 1/(\omega\alpha_0^{1/2})$.

By transforming away the fast oscillations in phase, one can construct an approximate invariant of the motion, known as the adiabatic invariant [7]. However, particles which trap or detrap cross the separatrix, a phase space trajectory of the time independent ($\varepsilon \to 0$) Hamiltonian separating bound and unbound trajectories. Because the separatrix contains a fixed point, particle oscillations in its vicinity are slow, causing a breakdown in adiabatic theory for all separatrix-crossing particles. This breakdown of adiabatic invariance occurs over the entire region of phase space where separatrix crossing occurs. We call this region separatrix-swept phase space.

Separatrix-crossing theory [8,9] provides an analytic description of the dynamics of separatrix-swept phase space. This theory uses the method of asymptotic matching to determine the adiabatic invariant after crossing a separatrix, given the adiabatic invariant before the crossing. Before and after the crossing, adiabatic invariance theory is used. Close to the separatrix, the change in the invariant is calculated perturbatively. The three solutions are then matched in the two regions of overlap. A calculation of this type was first performed by Timofeev [10] for a sinusoidal potential with slowly changing amplitude. The general 1D calculation was performed by Cary, Escande, and Tennyson [8], and independently by Neishtadt [11].

We define the ratio of the bounce time to the autocorrelation time to be the adiabaticity parameter. $\varepsilon_a = \varepsilon/\alpha^{1/2}$, where α is the local wave amplitude. The motion of trapped particles which remain far from any separatrix will be adiabatic if $\varepsilon_a \ll 1$. Separatrix-crossing theory can be applied to trajectories that trap or detrap if $\varepsilon/\alpha_x^{1/2} \ll 1$, where α_x is the wave amplitude at the time of trapping or detrapping. In other words, our analysis requires $\varepsilon_a \ll 1$ when the separatrix is crossed.

Previous studies [12,13] of the dynamical system considered here, which treated only a single wave-particle interaction for the limit $\varepsilon \to 0$, used adiabatic invariance theory and separatrix-crossing theory to explain the origin of strong particle scattering as follows. A nearly resonant particle with an initial momentum greater than the phase velocity of the wave will encounter the wave packet and become trapped, crossing the separatrix from above. This particle then oscillates inside the separatrix as it is ferried through the wave packet, until it detraps on the other side. Depending upon its phase, the particle will either detrap above the separatrix or below the separatrix. If it detraps above the separatrix, the final momentum of the particle when far from the wave will differ from its initial momentum only by $O(\varepsilon)$. If, however, the particle detraps below the separatrix, then its final momentum will differ by order unity from its initial momentum—this is the strong scattering that has previously been observed numerically. If the wave amplitude is large enough, some particles cross the separatrix twice in rapid succession from top to bottom (or vice versa) and are resonantly reflected by the wave. These issues are discussed at length in Ref. [13], which we will henceforth refer to as paper I.

The value of the adiabatic invariant after a separatrix-crossing depends very sensitively on a phase variable, called the crossing parameter M, which is linearly related to the angle conjugate to the adiabatic invariant. Given a trajectory which makes two successive separatrix crossings (e.g., trapping followed by detrapping), the crossing parameter at the second crossing will be correlated with the crossing parameter at the first crossing. The relationship between the two crossing parameters was calculated by Escande [14] for Hamiltonian systems containing symmetric separatrices, and independently by Cary and Skodje [9] for the general 1D case.

Thus, separatrix-crossing dynamics has been reduced to a map [8,9], which we call the separatrix-crossing map: after each crossing, the resulting values of J and M can be calculated for an arbitrary trajectory. In previous work, the authors [15] assumed the separatrix-crossing map to be stochastic (essentially, phase correlations between subsequent separatrix crossings were neglected) and used it to calculate a diffusion coefficient for resonant particle dynamics in a single wave with slowly, periodically modulated amplitude. Numerical results confirmed that the dynamics was diffusive, although phase correlations significantly altered the shape of the diffusion coefficient. The numerical work of Menyuk [16] indicates that, for a slowly and periodically driven standing wave, the trajectories of resonant particles move ergodically throughout separatrix-swept phase space, which further supports the hypothesis that the separatrix-crossing map is stochastic.

In addition, analytic work [17,18] has shown that separatrix-swept phase space is occupied by a homoclinic tangle, and that any stable islands within this tangle have areas which are $O(\varepsilon)$ or smaller. These results suggest that separatrix-swept phase space is ergodic in the limit $\varepsilon \to 0$. A region of phase space is called ergodic if the time average of any dynamical quantity, over long times, can be replaced by an ensemble average, with the ensemble uniformly distributed throughout the region in question [19]. Ergodicity of separatrix-swept phase space would unambiguously confirm that the separatrix-crossing map is stochastic. More importantly, given an arbitrary initial ensemble of particles in separatrix-swept phase space, ergodicity allows one to calculate analytically the average canonical momentum in the long-time limit.

We briefly present our Hamiltonian model in Sec. II

and discuss the necessity of transforming to a Hamiltonian which varies slowly as a function of position, with the particle position being treated as the independent variable. It is shown in this section how the separatrix divides phase space into three distinct regions. In Sec. III, we use adiabatic theory as formulated in Refs. [8] and [9] to calculate the adiabatic invariant through first order in ε, in each of the three regions of phase space. We also present the limiting forms of the lowest-order adiabatic invariant on the separatrix, and of the first-order corrected adiabatic invariant far from the wave packet.

We calculate the separatrix-crossing map for our Hamiltonian in Sec. IV, closely following Ref. [8] in calculating the change in the adiabatic invariant, and Ref. [9] in calculating the change in the crossing parameter between subsequent crossings. The many possible transitions from one phase space region to another are discussed in detail. (This issue is presented in a less compact but simpler and more geometrical fashion in paper I.) The Appendix treats the related problem of how to calculate the crossing parameter for the initial separatrix crossing.

In Sec. V, we impose periodicity on the system by placing our large-amplitude wave packet in a 1D box, and we discuss the long-time dynamics associated with multiple wave-particle interactions. Numerical results show that an initial particle ensemble will evolve dramatically during the first few wave-particle interactions, due to the strong scattering discussed above and in paper I. On a longer time scale, the dramatically altered distribution function relaxes slowly until it goes flat, with the particles now distributed uniformly (in a coarse-grained sense) throughout separatrix-swept phase space.

We summarize the salient aspects of our study in Sec. VI, where we also discuss the relevance of this work to specific physical problems. The applications considered include the dynamics of plasma electrons in the presence of strong, narrow-spectrum, electrostatic turbulence; high power rf current drive in a tokamak plasma; and the dynamics of electrons in a recirculating Compton-regime free-electron laser (FEL) with a wiggler magnet that is tapered at both ends so as to slowly ramp the magnetic field up and down.

II. HAMILTONIAN MODEL

We model the interaction between test particles and a 1D coherent wave packet using the following Hamiltonian:

$$H(q,p,t)=\tfrac{1}{2}p^2+\alpha(\varepsilon q)\cos(q-t)\ . \tag{1}$$

Units have been chosen such that the mass of the particle and the wave number and frequency of the wave are unity. The wave amplitude is assumed to have the form $\alpha(\varepsilon q)=\alpha_0 f(\varepsilon q)$, where f is a function of unit peak and unit width. The number of wavelengths within the wave envelope is given roughly by $1/\varepsilon \sim kL$, where k is the central wave number and L is the characteristic length scale of the wave packet; this number is large for a wave packet, implying that $\varepsilon \ll 1$. Trapped particles oscillate characteristically at the bounce frequency $\omega_b \equiv \alpha^{1/2}$. The value of the Hamiltonian function H is E, where E is the particle energy in the laboratory-frame (i.e., the frame where the wave envelope is stationary).

In dimensional units, the bounce time is $\tau_b \sim 1/(\alpha_0^{1/2}\omega)$, where ω is the wave frequency. The spectrum of wave numbers encompassed by the wave packet can be determined by Fourier transforming $\alpha(\varepsilon q)\cos(q-t)$; given the condition that $\varepsilon \ll 1$, one can obtain the relation $\Delta v_\phi \sim \omega/k^2L = \varepsilon\omega/k$. Thus we find that $\tau_{\text{auto}} \sim 1/(\varepsilon\omega)$, which in turn yields the ratio $\tau_b/\tau_{\text{auto}} \sim \varepsilon/\alpha^{1/2}$, our adiabaticiy parameter ε_a. We consider the parameter regime where $\varepsilon \ll 1$ and α_0 is of order unity, which implies that $\varepsilon_a \ll 1$ and $\tau_b \ll \tau_{\text{auto}}$.

It was shown in paper I that the Hamiltonian in Eq. (1) can be canonically transformed into the following Hamiltonian:

$$K(\phi,E,\lambda\equiv\varepsilon q)=-E\pm\sqrt{2[E-\alpha(\lambda)\cos(\phi)]}-\tfrac{1}{2}\ . \tag{2}$$

The value of the Hamiltonian function K is $-E_\phi$, where $E_\phi=(p-1)^2/2+\alpha(\lambda)\cos(q-t)$ is the particle energy in the wave frame (i.e., the frame where the wave oscillations are stationary). The new coordinate $\phi=q-t$ is the particle's phase with respect to the wave. The new canonically conjugate momentum E is the particle's energy in the laboratory frame. The new independent variable q is the particle's position.

The square root in Eq. (2) (including the $\pm$) is equal to p, the particle momentum in the lab frame. As is discussed in paper I, the fact that the Hamiltonian K has two branches leads to a phase space with two sheets; however, this phenomenon will cause us no difficulties. We show the phase space of the Hamiltonian for $\alpha=2$ in Fig. 1. Specifically, Fig. 1 shows contours of constant $K(\phi,E,\lambda)$, for a fixed value of λ, in the E-ϕ plane. One can imagine that the figure is wrapped around a vertical cylinder, so that $\phi=0$ and 2π are the same point. In Fig. 1, we have inverted the lower phase space sheet (where $p<0$) and attached it to the bottom of the upper sheet.

We have patched the two phase space sheets together

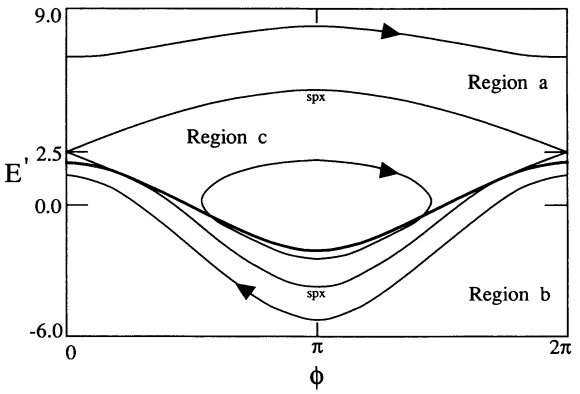

FIG. 1. Phase space of the Hamiltonian in Eq. (2) for $\lambda\equiv\varepsilon q$ held fixed and $\alpha(\lambda)=2$. The thicker line corresponding to $E'=\alpha(\lambda)\cos\phi$ divides the two phase space sheets. The two branches of the separatrix, labeled *spx*, divide the phase space into three regions: region *a* above the separatrix, region *b* below the separatrix, and region *c* inside the separatrix.

in Fig. 1 in order to show the phase space topology as clearly and simply as possible. However, this gives rise to a slight complication, because a given value of E does not uniquely correspond to one phase space sheet or another. For this reason, we introduce a variable E', such that $E'=E$ on the upper sheet, while $E'=2\alpha(\lambda)\cos(\phi)-E$ on the lower sheet. The thicker line in the figure, which corresponds to $E'=E=\alpha(\lambda)\cos(\phi)$, separates the two sheets.

In Fig. 1, the two branches of the separatrix are labeled *spx*. On these two curves, $E_\phi=\alpha(\lambda)$. The separatrix divides the phase space into three regions. We call the region above the separatrix region a, and trajectories in this region are said to be passing above. In region a, $p_\phi>0$ and $E_\phi>\alpha(\lambda)$, where $p_\phi=p-1$ is the wave-frame momentum. We call the region below the separatrix region b, and trajectories in this region are said to be passing below. In region b, $p_\phi<0$ and $E_\phi>\alpha(\lambda)$. We call the region inside the separatrix region c, where trajectories are trapped. In region c, p_ϕ can take either sign and $E_\phi<\alpha(\lambda)$.

III. ADIABATIC INVARIANCE THEORY

The adiabatic invariant J for a slowly varying 1D Hamiltonian of the form $K(\phi,E,\lambda\equiv\varepsilon q)=-E_\phi$ can be written as an asymptotic series in powers of ε:

$$J=J_0(E_\phi,\lambda)+\varepsilon J_1(E_\phi,\lambda,\phi)+\varepsilon^2 J_2(E_\phi,\lambda,\phi)+\cdots . \quad (3)$$

Kruskal [7] proved the existence of such a series for the general multidimensional problem, although specific 1D cases had been considered previously [20]. The lowest-order term J_0 is often called the action, which is the phase space area enclosed by a trajectory of the time-independent (i.e., $\varepsilon\to 0$) system. The first-order correction J_1 has been calculated for a number of specific cases [21,22] and for the general 1D problem [8,11].

It has been shown [9,23] that the successive terms in Eq. (3) arise naturally when transforming the slowly varying Hamiltonian, order by order in ε, to an integrable Hamiltonian. This is done by first transforming the Hamiltonian to action-angle variables, then using a series of near-identity canonical transformations to remove the angle dependence order by order in ε. The adiabatic invariant series is just the transformed action variable which results from this process, showing in a natural way that J is a canonical variable.

The action is defined by the equation

$$J_0(E_\phi,\lambda)\equiv\oint d\phi E_L(E_\phi,\lambda,\phi) , \quad (4a)$$

where $E_L(E_\phi,\lambda,\phi)$ is the function which satisfies the identity $K(\phi,E_L(E_\phi,\lambda,\phi),\lambda)=-E_\phi$ and which is equal in value to the canonical momentum E. Thus the function E_L is equal in value to our original Hamiltonian H, although it is a function of different variables. Inverting the Hamiltonian K yields

$$E_L(E_\phi,\lambda,\phi)=E_\phi+\tfrac{1}{2}\pm\sqrt{2[E_\phi-\alpha(\lambda)\cos(\phi)]} . \quad (4b)$$

The square root (including the $\pm$) is equal to p_ϕ, the particle momentum in the wave frame; the $+$ sign corresponds to the upper branch of E_L, and the $-$ sign to the lower branch.

The loop integral of Eq. (4a) is evaluated with E_ϕ and λ held fixed, and with ϕ changing in the direction of particle motion. (A different convention was used in paper I to simplify the exposition; however, we must use this convention here in order to apply the separatrix crossing theory of Ref. [8] in a straightforward manner.) In region a, the integration is from 0 to 2π and the upper branch of E_L is used, while in region b the integration is from 2π to 0 and the lower branch is used. In region c, the integral completes a full circuit in phase, using first one branch of E_L and then the other. These integrations yield

$$J_{0a}(E_\phi,\lambda)=8\alpha^{1/2}k^{-1}\mathcal{E}(k)+2\pi(E_\phi+\tfrac{1}{2}) , \quad (5a)$$

$$J_{0b}(E_\phi,\lambda)=8\alpha^{1/2}k^{-1}\mathcal{E}(k)-2\pi(E_\phi+\tfrac{1}{2}) , \quad (5b)$$

$$J_{0c}(E_\phi,\lambda)=16\alpha^{1/2}[\mathcal{E}(k^{-1})+(1-k^2)\mathcal{K}(k^{-1})] , \quad (5c)$$

$$k^2(E_\phi,\lambda)\equiv 2\alpha/(E_\phi+\alpha) , \quad (5d)$$

where $\mathcal{K}(k)$ and $\mathcal{E}(k)$ are complete elliptic integrals of the first and second kinds, respectively, as defined on p. 905 of Ref. [24]. The subscripts on J_0 indicate the phase space region for which the result is valid. These results differ from those in Eqs. (8) and (9) of paper I by a factor of 2π, a different sign convention, the addition of a constant to the invariants for regions a and b, and slightly different notation.

According to Eq. (B14) of Ref. [8], the first-order correction to the adiabatic invariant is

$$J_1(E_\phi,\lambda,\phi)=\frac{1}{2}\frac{\partial J_0(E_\phi,\lambda)}{\partial E_\phi}\frac{\partial J_0(E_\phi,\lambda)}{\partial\lambda}-\oint d\phi'\frac{\partial E_L(E_\phi,\lambda,\phi')}{\partial E_\phi}\times\int_\phi^{\phi'}d\phi''\frac{\partial E_L(E_\phi,\lambda,\phi'')}{\partial\lambda} . \quad (6a)$$

As was the case for J_0, this loop integral is evaluated with E_ϕ and λ held fixed, and with ϕ' and ϕ'' changing in the direction of particle motion, taking into account the two branches of E_L. We find it convenient to evaluate Eq. (6a) in each region of phase space at a particular value of ϕ, which we call ϕ_0. Then, once $J_1(E_\phi,\lambda,\phi_0)$ is known, we use Eq. (B9) of Ref. [8] to obtain J_1 for arbitrary ϕ:

$$J_1(E_\phi,\lambda,\phi)=J_1(E_\phi,\lambda,\phi_0)+\frac{\partial J_0}{\partial E_\phi}\int_{\phi_0}^{\phi}d\phi'\frac{\partial E_L(E_\phi,\lambda,\phi')}{\partial\lambda}-\frac{\partial J_0}{\partial\lambda}\int_{\phi_0}^{\phi}d\phi'\frac{\partial E_L(E_\phi,\lambda,\phi')}{\partial\lambda} . \quad (6b)$$

We choose $\phi_0=0,2\pi$ for passing trajectories, and $\phi_0=\phi_{\min}\equiv\arccos[E_\phi/\alpha(\lambda)]$ for trapped trajectories. We obtain the results

$$J_{1\beta}(E_\phi,\lambda,\phi)=\frac{4\alpha'}{\alpha}\{[\alpha^{1/2}\pi/k+\mathrm{sgn}(p_\phi)\mathcal{H}(k)][\mathcal{E}(\delta,k)-(1-k^2)\mathcal{F}(\delta,k)] -[\alpha^{1/2}\delta/k+\mathrm{sgn}(p_\phi)\mathcal{F}(\delta,k)][\mathcal{E}(k)-(1-k^2)\mathcal{H}(k)]\}\ , \tag{7a}$$

$$J_{1c}(E_\phi,\lambda,\phi)=-\frac{4\alpha'}{\alpha^{1/2}}\delta[2\mathcal{E}(k^{-1})-\mathcal{H}(k^{-1})]+\frac{8\alpha'}{\alpha}[\mathcal{E}(\gamma,k^{-1})\mathcal{H}(k^{-1})-\mathcal{E}(k^{-1})\mathcal{F}(\gamma,k^{-1})]\mathrm{sgn}(p_\phi)\ , \tag{7b}$$

where $\delta\equiv(\phi-\pi)$, $\gamma\equiv\arcsin[k\sin(\delta)]$, $\mathcal{F}(\gamma,k)$ and $\mathcal{E}(\gamma,k)$ are incomplete elliptic integrals of the first and second kinds as defined on pp. 904 and 905 of Ref. [24], and k is defined in Eq. (5d). The subscript β in Eq. (7a) is used to indicate that this result holds for both regions a and b. The function sgn has absolute value unity and takes the sign of its argument, while the symbol $'$ denotes differentiation with respect to λ.

Following paper I, we define the separatrix action $Y_\eta(\lambda)$ to be the value of the lowest-order adiabatic invariant on the separatrix in region η. Taking the limit $E_\phi\rightarrow\alpha(\lambda)$ of Eqs. (5), we obtain

$$Y_a(\lambda)=8\alpha^{1/2}+2\pi(\alpha+\tfrac{1}{2})\ , \tag{8a}$$

$$Y_b(\lambda)=8\alpha^{1/2}-2\pi(\alpha+\tfrac{1}{2})\ , \tag{8b}$$

$$Y_c(\lambda)=Y_a(\lambda)+Y_b(\lambda)=16\alpha^{1/2}\ . \tag{8c}$$

Again following paper I, we consider the form of the adiabatic invariant for passing particles far from the wave, where the local wave amplitude is vanishingly small. Taking the limit $\alpha\rightarrow0$ of Eqs. (5a) and (5b) yields

$$j_a(p)=\pi p^2\ , \tag{9a}$$

$$j_b(p)=-\pi p^2\ , \tag{9b}$$

where we have used a lower case j to indicate that this result holds only in the limit that the wave amplitude vanishes. Because momentum is conserved in this limit, it is reasonable that the adiabatic invariant should reduce to a simple function of the momentum. The results in Eqs. (8) and (9) differ from those presented in Eqs. (10) and (11) of paper I by a factor of 2π, a different sign convention, and the addition of a constant to the invariants for regions a and b.

IV. SEPARATRIX-CROSSING THEORY

In calculating the separatrix-crossing map for the Hamiltonian of Eq. (2), we use the following notation with regard to the three regions of phase space: the symbols α and β will each be used to refer to either region a or region b, but not region c, while the symbols ξ and η will be used to refer to any one of the three regions. In Sec. IV A, we closely follow Cary, Escande, and Tennyson [8] in calculating the required time-dependent parameters associated with near-separatrix motion and in presenting the formula for the change in J due to a single crossing. In Sec. IV B, closely following Cary and Skodje [9], we show explicitly how to calculate the change in the crossing parameter between trapping and detrapping, thus accounting for the effect of phase correlations.

A. A single separatrix crossing

To lowest order, the final adiabatic invariant of a separatrix-crossing trajectory can be determined simply by assuming that adiabatic invariance holds right up to the separatrix [8]. In that limit, the crossing occurs at the pseudocrossing time $\lambda_x=\varepsilon q_x$, defined by $J_{i\xi}\equiv Y_\xi(\lambda_x)$, where $J_{i\xi}$ is the initial value of J on the trajectory in region ξ. Likewise, if the trajectory crosses into region η, then the final value of the adiabatic invariant in that region is given, to lowest order, by $J_{f\eta}=Y_\eta(\lambda_x)$. In addition, the final value of J has a small phase-dependent correction, which we now proceed to calculate.

The period on a trajectory of the $\lambda=$const system is given by [8]

$$T_0(E_\phi,\lambda)=\frac{\partial J_0(E_\phi,\lambda)}{\partial E_\phi}=\oint d\phi\frac{\partial E_L(E_\phi,\lambda,\phi)}{\partial E_\phi}\ . \tag{10a}$$

If T_0 is evaluated and approximated for $|E_\phi-\alpha(\lambda)|\ll1$ (i.e., near the separatrix), it takes the following form:

$$T_{0\beta}(E_\phi,\lambda)=\omega_b^{-1}\ln|E_{\phi\beta}/(E_\phi-\alpha)| +O((E_\phi-\alpha)\ln|E_\phi-\alpha|)\ , \tag{10b}$$

$$T_{0c}(E_\phi,\lambda)=2\omega_b^{-1}\ln|E_{\phi c}/(E_\phi-\alpha)| +O((E_\phi-\alpha)\ln|E_\phi-\alpha|)\ , \tag{10c}$$

where the energy parameters are given by

$$E_{\phi a}=32\alpha\exp(2\pi\alpha^{1/2})\ , \tag{11a}$$

$$E_{\phi b}=32\alpha\exp(-2\pi\alpha^{1/2})\ , \tag{11b}$$

$$E_{\phi c}=(E_{\phi a}E_{\phi b})^{1/2}=32\alpha\ , \tag{11c}$$

and $\omega_b=\alpha^{1/2}$ is the exponentiation rate of orbits near the saddle point.

The change in the value of the Hamiltonian during one near-separatrix oscillation, denoted by $\Delta E_{\phi\eta}$, is used in the definition of the crossing parameter. To first order in ε, we obtain [8]

$$-\Delta E_{\phi a}(\lambda)=\dot{Y}_a(\lambda)=\varepsilon\frac{4\alpha'}{\alpha^{1/2}}(1+v)\ , \tag{12a}$$

$$-\Delta E_{\phi b}(\lambda)=\dot{Y}_b(\lambda)=\varepsilon\frac{4\alpha'}{\alpha^{1/2}}(1-v)\ , \tag{12b}$$

$$-\Delta E_{\phi c}(\lambda)=\dot{Y}_c(\lambda)=\varepsilon\frac{8\alpha'}{\alpha^{1/2}}\ , \tag{12c}$$

where we define $v\equiv(\pi/2)\alpha^{1/2}$. Near the separatrix, E_ϕ changes by the same amount in region c during the upper half of a trapped oscillation as it does during a single oscillation in region a. Likewise, near the separatrix, E_ϕ

changes by the same amount in region c during the lower half of a trapped oscillation as it does during a single oscillation in region b. This is the reason that $\Delta E_{\phi c}=\Delta E_{\phi a}+\Delta E_{\phi b}$. We also define the parameters

$$R_a(\lambda)\equiv \dot{Y}_a/\dot{Y}_c=\tfrac{1}{2}(1+v)\ , \tag{13a}$$

$$R_b(\lambda)\equiv \dot{Y}_b/\dot{Y}_c=\tfrac{1}{2}(1-v)\ , \tag{13b}$$

which provide a more compact notation.

We define a vertex in regions a and b to be an intersection of a phase space trajectory with the line $\phi=0$. In region c, we define a vertex to be any turning point of a trajectory. At a turning point, $dE/dq=-\partial K/\partial\phi$ goes to infinity—this occurs when $\phi=\phi_{\min}$ and when $\phi=\phi_{\max}\equiv 2\pi-\phi_{\min}$. The critical vertex is defined to be the first, last, or only vertex in region c during the separatrix-crossing process. There can be only one such vertex [8]. Following Ref. [8], we define the crossing parameters to be

$$M_a\equiv[E_{\phi 0}-\alpha(\lambda_x)]/\Delta E_{\phi a}(\lambda_x)\ , \tag{14a}$$

$$M_b\equiv[E_{\phi 0}-\alpha(\lambda_x)]/\Delta E_{\phi b}(\lambda_x)\ , \tag{14b}$$

$$M_c\equiv[E_{\phi 0}-\alpha(\lambda_x)]/\Delta E_{\phi c}(\lambda_x)\ , \tag{14c}$$

where $E_{\phi 0}$ is the value of the Hamiltonian at the critical vertex. The possible range of crossing parameters will be discussed below in Sec. IV B. It is shown in the Appendix how to calculate the crossing parameter, given arbitrary initial phase space coordinates.

There is another parameter G, defined below Eq. (64c) of Ref. [8], which is related to the value of J_1 at a vertex. It was shown in Ref. [8] that, near the separatrix, J_1 can be found to lowest order at a vertex in region a or b simply by evaluating it at the saddle point. It can be determined from Eq. (7a) above that J_1 vanishes at the saddle point in regions a and b. Thus the parameters g_a and g_b, defined in Eq. (26) of Ref. [8], vanish for our system, which means the parameter G also vanishes.

Now we can present the equations for the final values of J after a separatrix crossing. If the transition is from region α to region c (or vice versa), then the final value of the adiabatic invariant in region η is given by [8]

$$J_{f\eta}=Y_\eta+\frac{\dot{Y}_\eta}{\omega_b}[\ln|\Gamma(-|M_\alpha|)\Gamma(1+R_\alpha|M_\alpha|)\Gamma(1-R_\alpha+R_\alpha|M_\alpha|)/(2\pi)^{3/2}|$$
$$+\ln|E_{\phi c}/E_{\phi\alpha}|+(\tfrac{1}{2}+|M_\alpha|)\ln|E_{\phi\alpha}/\dot{Y}_\alpha|-(1-R_\alpha+2R_\alpha|M_\alpha|)\ln|E_{\phi c}/\dot{Y}_c|]\ . \tag{15a}$$

If the transition is from region α to region β, the final value of the adiabatic invariant is [8]

$$J_{f\beta}=Y_\beta+\frac{\dot{Y}_\beta}{\omega_b}[\ln|\Gamma(1+M_\beta)\Gamma(1-M_\alpha)/2\pi|-\tfrac{1}{2}\ln|M_\alpha M_\beta|+M_\alpha\ln|E_{\phi\alpha}/\dot{Y}_\alpha|-M_\beta\ln|E_{\phi\beta}/\dot{Y}_\beta|]\ . \tag{15b}$$

In Eqs. (15), Γ is the complete gamma function, as defined on p. 933 of Ref. [24], $\omega_b=\alpha^{1/2}$ is the exponentiation rate of orbits near the saddle point, and all the time-dependent quantities are to be evaluated at the pseudo-crossing time λ_x.

B. Phase correlations between subsequent crossings

We now use the results of Ref. [9] to calculate the change in the crossing parameter for a trajectory which traps into region c, then subsequently detraps. First we define the necessary quantities, then we present the general formula. Finally, we show explicitly how the formula is implemented for our system.

The crossing parameter is linearly related to the adiabatic angle [8] (i.e., the angle canonically conjugate to the adiabatic invariant series), so calculating its change involves a time integral of the adiabatic frequency. Because the integration time will be of order ε^{-1} (i.e., the time between successive separatrix crossings), the adiabatic frequency must be calculated through order ε in order to obtain a result correct through order unity. The first-order corrected frequency $\nu^1(J^1,\lambda)$ is obtained by differentiating the first-order corrected Hamiltonian with respect to the first-order corrected invariant, $J^1(E_\phi,\lambda,\phi)\equiv J_0(E_\phi,\lambda)+\varepsilon J_1(E_\phi,\lambda,\phi)$.

First we define the lowest-order Hamiltonian $K_0(J_0,\lambda)$ as the inverse of the function $J_0(E_\phi,\lambda)$:

$$J_0(K_0(x,\lambda),\lambda)\equiv x\ . \tag{16a}$$

Thus K_0 has the same numerical value as the Hamiltonian given in Eq. (2), but will have a different functional form. In fact, we define K_0 only implicitly through Eq. (16a), because we cannot invert Eqs. (5) analytically. The lowest-order frequency is

$$\nu_0(J_0,\lambda)=\frac{\partial K_0(J_0,\lambda)}{\partial J_0}=\left[\frac{\partial J_0(K_0(J_0,\lambda),\lambda)}{\partial E_\phi}\right]^{-1}\ , \tag{16b}$$

where the second equality follows from taking the partial derivative of both sides of (16a) with respect to x, then letting $x=J_0$.

Using Eqs. (9) and (11) of Ref. [9], we find the first-order corrected Hamiltonian:

$$K^1(J^1,\lambda)=K_0(J^1,\lambda)$$
$$-\varepsilon\nu_0(J^1,\lambda)$$
$$\times J_1[K_0(J^1,\lambda),\lambda,\phi_0(K_0(J^1,\lambda),\lambda)]\ . \tag{17a}$$

Here $K_0(J^1,\lambda)$ and $\nu_0(J^1,\lambda)$ are the functions defined in Eqs. (16), with the first-order corrected adiabatic invari-

ant $J^1 \equiv J_0 + \varepsilon J_1$ used in place of J_0. Similarly, $J_1(K_0,\lambda,\phi_0)$ is the first-order correction to the adiabatic invariant as defined in Eqs. (7), but with the indicated arguments replacing the original ones. We choose $\phi_0(K_0(J^1,\lambda),\lambda)=0$ in regions a and b, and $\phi_0=\phi_{\min}\equiv\arccos(E_\phi/\alpha)$ in region c. We obtain the first-order corrected frequency by differentiating Eq. (17a) with respect to J_1:

$$\nu^1(J^1,\lambda)=\nu_0(J^1,\lambda)-\varepsilon\left[\frac{\partial\nu_0(J^1,\lambda)}{\partial J^1}J_1(K_0,\lambda,\phi_0)+\nu_0(J^1,\lambda)\frac{\partial J_1(K_0,\lambda,\phi_0)}{\partial J^1}\right]. \tag{17b}$$

Because the final phase space is symmetric about the line $\phi=\pi$, $J_{1\alpha}(E_\phi,\lambda,\phi=0)$ vanishes. Thus, the $O(\varepsilon)$ term on the right-hand side of Eqs. (17) is nonzero only in region c.

We defined the critical vertex in Sec. IV A to be the first, last, or only vertex in region c. This means, as can be seen from Fig. 1, that the critical vertex may lie on the left ($\phi<\pi$) or the right side ($\phi>\pi$) of the phase space. It is necessary to define a crossing parameter M_r, which is a crossing parameter for region c that is calculated using $E_{\phi r}$, the value of the Hamiltonian at the first or last vertex to the right of the line $\phi=\pi$:

$$M_r \equiv E_{\phi r}/\Delta E_{\phi c}(\lambda_x)\ . \tag{18}$$

It is not necessary to define M_r for transitions from region a to b, or vice versa, for which the critical vertex is the only vertex in region c. Depending on the transition taking place, either $M_c=M_r$, $M_c=M_r-R_a$, or $M_c=M_r+R_b$. The crossing parameter M_r is equivalent to the parameter M_u defined in Ref. [8].

Table I gives the range of the relevant crossing parameters for every possible transition. The top half of Table I considers the case $\alpha'(\lambda_x)>0$, which means any transitions must take place on the left side of the wave, while the bottom half of the table considers the case $\alpha'(\lambda_x)<0$, which means any transitions must take place on the right side of the wave. The bottom and top halves of the table are each broken into two sections—one for which $R_b(\lambda_x)>0$, and one for which $R_b(\lambda_x)<0$.

The first row of Table I considers trajectories that are initially in phase space region a. One can see from the first two entries in this row that it deals with the case $\alpha'(\lambda_x)>0$ and $R_b(\lambda_x)>0$ [i.e., $v(\lambda_x)\le 1$]. Because the critical vertex is in region c, we know that $[E_{\phi 0}-\alpha(\lambda_x)]<0$. Furthermore, $[E_{\phi 0}-\alpha(\lambda_x)]-\Delta E_{\phi a}>0$, because the previous vertex was in region a. These last two inequalities, upon dividing by the positive quantity $-\Delta E_{\phi a}$, are expressed in the third entry of the row. The fact that $\Delta E_{\phi a}$ is negative is consistent with Eq. (12a) for positive α'. We note that if $\Delta E_{\phi b}$ were positive, then those separatrix-crossing trajectories closest to the lower branch of the separatrix would immediately detrap into region b; however, Eq. (12b) indicates that $\Delta E_{\phi b}<0$ for α' and R_b both positive, so all the separatrix-crossing trajectories remain in region c. This result is expressed in the fourth entry of the row. Because the critical vertex occurs to the right of the line $\phi=\pi$ for an $a\to c$ transition, $M_r=M_c$, and the fifth entry in the row is obtained from the definitions of M_a and M_c given in Eqs. (14). The sixth entry in the row is obtained directly from the third and fifth entries. The other rows in Table I were obtained by similar analyses.

If a trajectory crosses the separatrix into region c at the pseudocrossing time λ_x and with crossing parameter M_r, then at some later time leaves region c, we call the second crossing time λ_x' and the second crossing parameter M_r'. Similar notation is used for trajectories that enter and exit region a or b.

The resulting crossing parameter is given in terms of the old one by Eqs. (37) of Ref. [9]:

TABLE I. For the sign of α' given in the first column and the sign of R_b given in the second column, if the crossing parameter in the initial region is in the range indicated in the third column, then the transition given in the fourth column takes place. The fifth column gives the crossing parameter relevant to the new region, and the sixth column gives its range. All possible separatrix-crossing transitions are shown.

$\alpha'(\lambda_x)$	$R_b(\lambda_x)$	Initial region: range of crossing parameter	Resulting transition	New region: crossing parameter	Range of new crossing parameter
$\alpha'>0$	$R_b>0$	$0<M_a<1$	$a\to c$	$M_r=M_aR_a$	$0<M_r<R_a$
		$0<M_b<1$	$b\to c$	$M_r=M_bR_b+R_a$	$R_a<M_r<1$
	$R_b<0$	$0<M_a<-R_b/R_a$	$a\to b$	$M_b=M_aR_a/R_b$	$-1<M_b<0$
		$-R_b/R_a<M_a<1$	$a\to c$	$M_r=M_aR_a$	$-R_b<M_r<R_a$
$\alpha'<0$	$R_b>0$	$-1<M_r<-R_b$	$c\to a$	$M_a=(M_r+R_b)/R_a$	$-1<M_a<0$
		$-R_b<M_r<0$	$c\to b$	$M_b=M_r/R_b$	$-1<M_b<0$
	$R_b<0$	$-1<M_r<0$	$c\to a$	$M_a=(M_r+R_b)/R_a$	$-1<M_a<-R_b/R_a$
		$0<M_b<1$	$b\to a$	$M_a=M_bR_b/R_a$	$-R_b/R_a<M_a<0$

$$M_r' = \mathrm{frac}\{M_r + \Phi_c(J_m) + \tfrac{1}{4}[R_b(\lambda_x) - R_a(\lambda_x) - R_b(\lambda_x') + R_a(\lambda_x')]\} - 1 , \quad (19a)$$

$$M_\alpha' = \mathrm{frac}[M_\alpha + \Phi_\alpha(J_m)] , \quad (19b)$$

where frac is a function which yields the fractional part of its argument, and J_m is the value of J^1 between the two separatrix crossings. The subtraction of unity at the end of Eq. (19a) puts M_r' in the proper interval. As can be seen from the third column of Table I, the value of M_r' must lie in the interval $(-1,0)$ before a transition takes place, while M_α' must lie in the interval $(0,1)$. The phase advance function $\Phi_\eta(J_m)$ is defined by

$$\Phi_\eta(J_m) \equiv \varepsilon^{-1} \int_{\lambda_x}^{\lambda_x'} d\lambda \, \nu_\eta^1(J_m, \lambda) , \quad (19c)$$

with J_m held constant during the integration. In general, this integral must be evaluated by quadrature.

We defined the pseudocrossing time in Sec. IV A in terms of the value of J on the trajectory and the value of the separatrix action in the initial region. In Eqs. (19), λ_x' is defined in just this way; however, the λ_x in these equations is defined in terms of J_m. To be more explicit, we have $J_m \equiv Y_\eta(\lambda_x') \equiv Y_\eta(\lambda_x)$. Equations (15) and (19) constitute a map for our system—the separatrix-crossing map.

C. Comparison of theory with numerics

We consider an initial ensemble of trajectories far to the left of the wave in phase space region a, each with the same momentum p_i and uniformly distributed in the adiabatic angle. We wish to use separatrix-crossing theory to predict the final momentum of each particle long after its interaction with the wave p_f, and compare these results with those obtained by numerically integrating the equations of motion.

In Fig. 2, we plot the final momentum p_f versus the initial adiabatic angle Θ_{ia}. The initial phases of the particles were chosen so that the values of M_a at the first crossing would be uniformly distributed between 0 and 1. (We explain in the Appendix how to do this.) The initial adiabatic invariant is $J_{ia} = 8.14$ ($p_i \approx 1.61$); the maximum wave amplitude is $\alpha_0 = 0.4$; and the slowness parameter ε is equal to (a) 0.04, (b) 0.02, and (c) 0.001.

The solid lines in Fig. 2 were obtained by using separatrix-crossing theory as described in Secs. IV A and IV B, to find the final value of the adiabatic invariant in region α, $J_{f\alpha}$. The final momentum was then obtained from Eq. (9). The dotted lines simply show the breaks between initial conditions which result in detrapping into region a and those that result in detrapping into region b. The squares show the results of numerically integrating the equations of motion.

The horizontal dashed lines in Figs. 2(a) and 2(b) show the two possible values of p_f according to the lowest-order dynamics discussed in paper I. The upper line is just $p_f = p_i$, while the lower line is given by Eq. (13) of paper I. Figures 2(a) and 2(b) indicate that the agreement between theory and numerics improves as ε is decreased from 0.04 to 0.02. In Fig. 2(c), we show only those particles that detrapped into region a, with $\varepsilon = 0.001$. This figure indicates that, as ε becomes very small, the separatrix-crossing map is able to reproduce virtually every detail of the particle dynamics. We note that the discrepancy between theory and numerics seen in Fig. 2(a) is primarily in the phase, which suggests that phase-averaged quantities obtained from the separatrix-crossing map would be accurate for ε as large as 0.04.

Given an ensemble of resonant trajectories with the same adiabatic invariant and uniformly distributed in the adiabatic angle over the unit interval, the fraction which is finally in one beam or another can be determined in a straightforward manner from Table I of Sec. IV B. As an example, we consider α_0 to be in the large-amplitude regime, first with an ensemble initially to the left of the wave, then with an ensemble initially trapped.

If the resonant ensemble is initially to the left of the wave in region a or b, then one can see from the first two

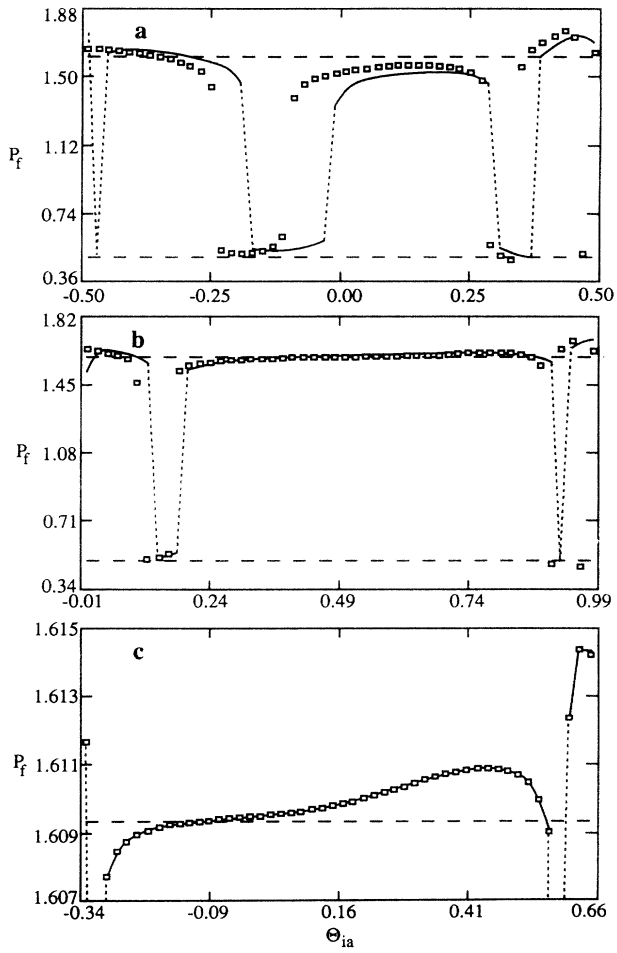

FIG. 2. A plot of the final momentum far to the right of the wave, p_f vs the initial adiabatic phase far to the left of the wave, Θ_{ia}. The slowness parameter is (a) $\varepsilon = 0.04$, (b) $\varepsilon = 0.02$, and (c) $\varepsilon = 0.001$, with $\alpha_0 = 0.4$ in every case. The horizontal dashed lines gives the values of p_f predicted in the limit $\varepsilon \to 0$. The solid lines were obtained using the full separatrix-crossing map. The squares are the results of numerical simulations.

rows of Table I that if $R_b(\lambda_x)>0$, all of the trajectories trap in the wave and none are reflected. If the ensemble is initially to the left of the wave in region a, and if $R_b(\lambda_x)<0$, then one can see from the third column of the third and fourth rows that the fraction of trajectories that trap is $F_T=1+R_b(\lambda_x)/R_a(\lambda_x)$, and the fraction of trajectories that reflect is $F_R=-R_b(\lambda_x)/R_a(\lambda_x)$. We can summarize these results by writing

$$F_T=\begin{cases}1 \text{ for } 0<v_x<1 & \text{(20a)}\\ \dfrac{1-v_x}{1+v_x} \text{ for } v_x>1\ , & \text{(20b)}\end{cases}$$

$$F_R=1-F_T\ , \qquad \text{(20c)}$$

where we have used Eqs. (13), and $v_x\equiv v(\lambda_x)$.

If the ensemble is initially in region c (i.e., trapped), and if $R_b(\lambda_x)>0$, then one can see from the third column of the fifth and sixth rows of Table I that the fraction of trajectories that detrap into region a is $F_a=R_a(\lambda_x)=1-R_b(\lambda_x)$, and the fraction of trajectories that detrap into region b is $F_b=R_b(\lambda_x)$. For $R_b(\lambda_x)<0$, we can see from the seventh row that all of the trajectories detrap into region a. We summarize these results as follows:

$$F_a=\begin{cases}\frac{1}{2}(1+v_x) \text{ for } 0<v_x<1 & \text{(21a)}\\ 1 \text{ for } v_x>1\ , & \text{(21b)}\end{cases}$$

$$F_b=1-F_a\ , \qquad \text{(21c)}$$

where we have once again used Eqs. (13). Probabilities of this type have been previously calculated for separatrix-crossing problems (see, e.g., Ref. [8] and references therein).

We compare these analytic results, which hold in the limit $\varepsilon\to 0$, with the results of numerical simulations in Fig. 3 by plotting F_T, F_R, F_a and F_b vs the quantity v_x, for $\alpha_0=3$ and $\varepsilon=0.07$. In this figure, v_x increases from zero both to the left and to the right. The values of v_x to the left of zero correspond to ensembles which were initially in region b, while those to the right of zero correspond to ensembles that were initially in region a.

The numerical data in Fig. 3, represented by open and filled squares, were obtained by the following method. First, an initial value of the adiabatic invariant, $J_{i\alpha}$, was chosen such that v_x would have the desired value. This was done by using the definition of v to solve for α_x, then using Eqs. (8a) and (8b) to solve for $Y_\alpha(\lambda_x)$, and finally letting $J_{i\alpha}=Y_\alpha(\lambda_x)$. Second, 3×10^3 initial conditions with this value of $J_{i\alpha}$ were placed far to the left of the wave in region α, uniformly distributed in the adiabatic angle $\Theta_{i\alpha}$ over the unit interval. Third, the equations of motion were integrated until each particle had interacted with the wave and was again far from the wave.

The vertical positions of the open squares in Fig. 3(a), which indicate the fraction of particles that become trapped, were obtained by counting the number of particles that were finally to the right of the wave, and dividing by the total number of particles. The vertical positions of the filled squares, which indicate the fraction of particles that become reflected, are obtained (by definition) by reflecting the open squares about the $F_T=0.5$ line.

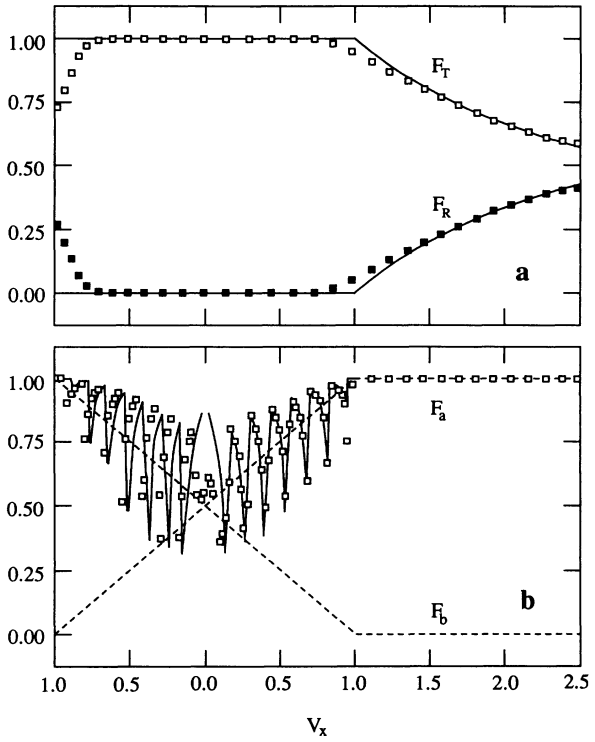

FIG. 3. In (a), the trapping fraction of an initial ensemble uniformly distributed in the adiabatic angle over the unit interval, F_T, and the reflecting fraction $F_R=1-F_T$ are plotted vs the parameter $v_x=(\pi/2)\alpha^{1/2}(\lambda_x)$. The solid lines were obtained from Eqs. (20), and the symbols were obtained by numerically integrating 3×10^3 trajectories through the wave. In (b), the fraction of trapped particles which detraps into region a, F_a, is plotted vs v_x. The dashed lines show F_a and $F_b=1-F_a$ as given by Eqs. (21). The solid line shows F_a as given by the full separatrix-crossing map. The squares were obtained from the same numerical simulations used for (a). In both plots, $\varepsilon=0.07$ and $\alpha_0=3$.

The vertical positions of the open squares in Fig. 3(b), which indicate the fraction of trapped particles that detrap into region a, were obtained by counting the number of particles with final momentum p_f such that $p_f>1$, then dividing by the total number of particles that were finally to the right of the wave. In order to avoid excessive clutter, we do not show the results for particles that detrap into region b, which can be obtained by reflecting the open squares about the $F_a=0.5$ line. Because 3×10^3 initial conditions were used in each case, the statistical error in the vertical positions of the squares should be on the order of a few percent.

The solid lines in Fig. 3(a) were obtained from Eqs. (20). Comparing these lines with the numerical data shows that theory predicts F_T and F_R to a good approximation for most values of v_x, even with ε as large as 0.07. However, the numerical data for ensembles initially in re-

gion b (data for these ensembles appear toward the left edge of the plot), and for v_x close to unity, do not agree well with the theory, which indicates that all trajectories should become trapped. Particles for which $p_i < 1$ and $v_x \lesssim 1$ are within the resonant or separatrix-crossing regime to lowest order in ε and, hence, should trap, but they are very close to the ponderomotive reflection regime [13]. Of such particles, those that reflect do so because, as they approach the separatrix very closely, their adiabatic invariant changes by $O(\varepsilon)$, which is enough to move them into the ponderomotive regime. This issue is discussed in greater detail in paper I.

The dashed lines in Fig. 3(b) were obtained from Eqs. (21), which assume that the ensemble is uniformly distributed in the adiabatic angle before the separatrix crossing occurs. We refer to this as the random-phase assumption. However, the ensembles used in our simulations were not uniformly distributed in the adiabatic angle before detrapping from the wave. Instead, each ensemble had some nontrivial distribution in phase as a result of the separatrix crossing that occurred when the particles became trapped.

The solid line in Fig. 3(b) shows the theoretical prediction for F_a as a function of v_x, taking the effect of correlations (i.e., the nonuniformity of the phase distribution) into account. For the sake of clarity, we do not show the result for F_b, which is obtained by reflecting the result for F_a about the $F_a = 0.5$ line. The solid line exhibits strong oscillations about the random-phase prediction. These oscillations are similar to those shown in Fig. 11 of Ref. [9] for the symmetric double-well potential.

A comparison of the solid line and the open squares in Fig. 3(b) shows the separatrix-crossing theory predicts F_a (and, hence, F_b as well) to a reasonable approximation for many values of v_x, even for ε as large as 0.07. For the ensembles initially in region b, there is a phase shift between the theory and the simulations, although qualitative agreement is obtained. In particular, the number of oscillations about the random-phase prediction is the same for both. If ε were decreased, the agreement between theory and numerics in Fig. 3(b) would improve; however, the number of oscillations of F_a around the random-phase prediction increases with ε^{-1}. Thus it becomes difficult to make a plot like Fig. 3(b) in the limit of small ε.

For $v_x \ll 1$, the theoretical prediction does not agree even qualitatively with the numerical simulations. This is because the adiabaticity parameter $\varepsilon_a \equiv \varepsilon/\alpha^{1/2}$ diverges at the time of trapping for any finite value of ε (even if $\varepsilon \ll 1$) in the limit that $\alpha_x \to 0$ or, equivalently, in the limit $p_i \to 1$. We call this the exact resonance limit, because it corresponds to the initial velocity of the particle approaching the phase velocity of the wave.

The separatrix-crossing map breaks down in the exact resonance limit, because separatrix-crossing theory requires that the rate of change of the Hamiltonian, ε, be small compared to the exponentiation rate of orbits near the fixed point at the time that the separatrix is crossed, $\alpha_x^{1/2}$ (hence our requirement that ε_a be small during trapping and detrapping). Furthermore, trajectories that trap when the wave amplitude is very small will oscillate only very slowly, even after they are far from the separatrix, because the maximum bounce frequency in the wave (i.e., that for deeply trapped particles) is $\alpha^{1/2}$; thus the assumption of a separation in time scales is violated and adiabatic invariance theory will not be valid subsequent to the separatrix crossing. This in turn violates the requirement of separatrix-crossing theory that trajectories be adiabatic before and after the separatrix is crossed. The dynamics of particles that trap and detrap in the exact resonance limit remains an open problem.

V. MULTIPLE WAVE-PARTICLE INTERACTIONS

FKRB present an extensive study of multiple wave-particle interactions in a system very similar to ours, finding diffusive dynamics in the weak turbulence limit, while showing the dynamics in the strong turbulence limit to be dominated by strong scattering. Here we further clarify the dynamics of the strong turbulence limit by applying separatrix-crossing theory. Our model consists of a wave packet in a one-dimensional box of length L_B, where L_B is much larger than the scale length of the wave envelope, as is shown in Fig. 4, with $\alpha_0 = 0.3$, $\varepsilon = 0.05$, and $L_B = 500$. Trajectories which exit the box to the left or right simply enter at the other side with the same momentum. This configuration corresponds to a periodic array of wave packets, which means that the Hamiltonian of Eq. (2) is now periodic in the slow "time" variable $\lambda \equiv \varepsilon q$.

Because the velocity of resonant particles (in our di-

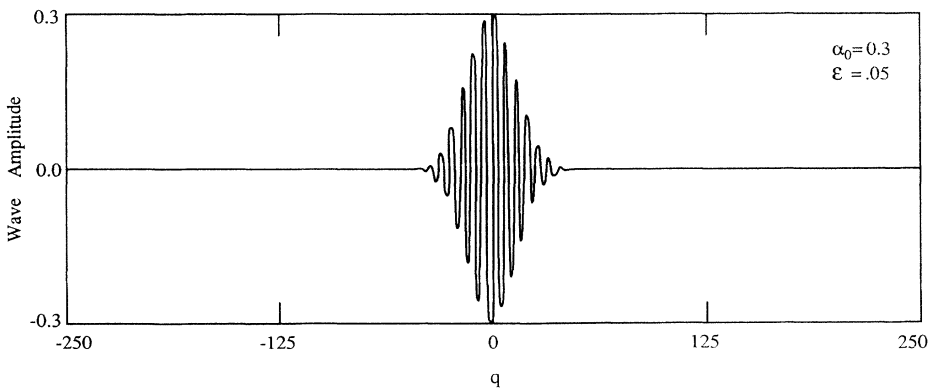

FIG. 4. Wave packet, with $\alpha_0 = 0.3$ and $\varepsilon = 0.05$, in a one-dimensional box of length $L_B = 500$, with periodic boundary conditions.

mensionless units) is of order unity, the time scale associated with wave-particle interactions in our box is $T_s = O(L_B)$. If the initial distribution is a single cold beam, then the distribution after a few wave-particle interactions will be two warm beams. For longer times, the dynamics will be dominated by diffusive effects. The time required for an arbitrary initial ensemble to fill separatrix-swept phase space sets the time scale associated with diffusion, T_d. It was shown in Ref. [8] that the small phase-dependent kick for a given particle is $O(\varepsilon \ln|\varepsilon^{-1}|)$, which implies that the mean square spreading of an ensemble due to each interaction must be $O(\varepsilon^2 \ln^2|\varepsilon|)$. The size of separatrix-swept phase space is of order unity, and the time between wave-particle interactions is $O(L_B)$, so the time for an arbitrary ensemble to saturate is roughly $T_d = O(L_B/\varepsilon^2 \ln^2|\varepsilon|)$. See Ref. [15] for a detailed discussion of the time scale for spreading throughout separatrix-swept phase space. In the limit of small ε, $T_d \gg T_s$, and the two time scales are well separated.

Previous numerical and analytic work suggests that trajectories move ergodically throughout separatrix-swept phase space [15–18]. If this is correct, then any trajectory which is initially in separatrix-swept phase space will eventually come arbitrarily close to every point in that region. After a long time, the probability of finding such a trajectory in any localized region within separatrix-swept phase space is simply proportional to the area of that region, independent of the trajectory's initial conditions.

Given an arbitrary initial ensemble of trajectories in separatrix-swept phase space, after many separatrix crossings they will reach a steady state in which their final distribution is approximately uniform throughout this entire phase space region. Thus, for the wave-packet potential, an arbitrary initial ensemble of trajectories will eventually become uniform in the (ϕ,E) phase space at fixed λ (i.e., at fixed q). The transformation from the Hamiltonian of Eq. (1) to the Hamiltonian of Eq. (2) was canonical, so this steady-state ensemble will also be uniform in (q,p) phase space at fixed t (i.e., the real time). In simpler terms, the momentum distribution function eventually goes flat.

The dynamical scenario we have just described is verified by the numerical results presented in Fig. 5, which shows the time evolution of the momentum distribution function, $F(p)$, 5×10^3 particles and the system parameters $\alpha_0=0.3$, $\varepsilon=0.05$, and $L_B=500$. The top frame shows the initial beam of particles with $p_i=0.525$. The particles were randomly distributed in phase, but closely packed, and far from the wave.

In the second frame in Fig. 5, we see $F(p)$ at the time $t=1000$, after which some of the particles have interacted with the wave twice and some only once. Most of the particles have been kicked into the higher momentum beam. The value of this higher momentum (in the limit $\varepsilon\to0$) is predicted by Eq. (13) of paper I to be $p_f\approx1.57$.

The third frame of Fig. 5 shows the distribution function for $t=5000$, or after approximately ten wave interactions for each particle. The two beams have by this time become roughly equal in intensity and have spread

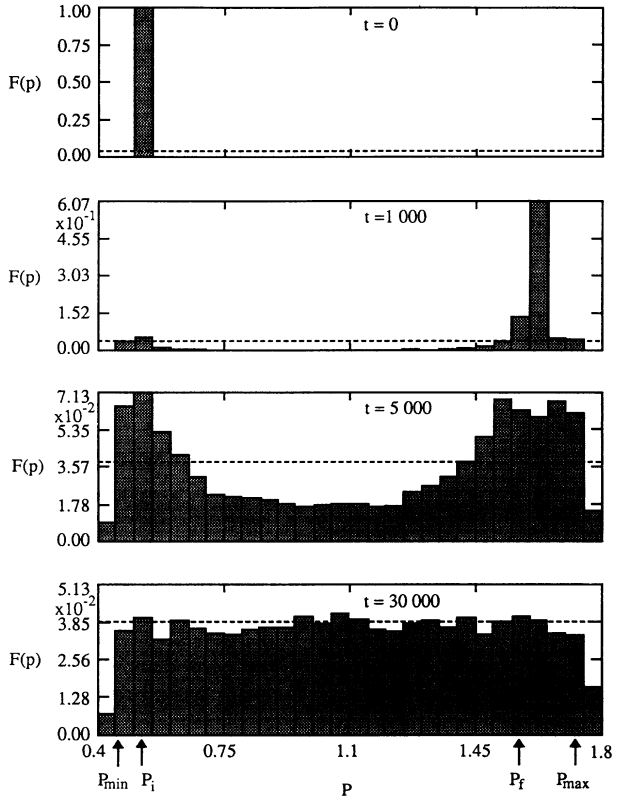

FIG. 5. Time evolution of the momentum distribution function $F(p)$ for 5×10^3 test particles interacting with the wave packet shown in Fig. 4.

over all of the possible momentum values. We see in the bottom frame of Fig. 5 that, after an average of about 60 wave interactions for each particle ($t=3\times10^4$), the momentum distribution function is essentially flat.

In each frame of Fig. 5, the 5×10^3 particles were binned according to their momentum, with 26 bins between $p_{\min}\approx0.453$ and $p_{\max}\approx1.73$ [see Eqs. (14) of paper I]. In the limit that the wave width ε^{-1} is small compared to the periodicity length L_B, most of the particles should be uniformly distributed in momentum between $p_{\min}$ and $p_{\max}$. Therefore, the fraction of particles in each of the 26 bins between these momentum values should be $1/26\approx3.85\times10^{-2}$, which is roughly what we see in the bottom frame of Fig. 5.

Given that the dynamics of this system is ergodic, it is straightforward to calculate the average momentum of an ensemble of resonant particles in the long-time limit. Explicit formulas have been calculated previously [25], but here we wish to emphasize the general utility of this idea rather than the specific details for our simple model. Such a calculation would be of great interest, for example, in the case of very strong rf current drive (discussed in Sec. VI), for which it would allow one to obtain analytically the achieved current as a function of system parameters.

VI. DISCUSSION

We have shown how separatrix-crossing theory can be applied to 1D accelerating structures with slow spatial

variation, such as a broad wave packet. We have calculated the adiabatic invariant series J through first order in the slowness parameter ε. When the wave amplitude is of order unity, there exists a large class of resonant trajectories which either trap in the wave and subsequently detrap, or else are resonantly reflected by the wave. The adiabatic invariant is broken along such trajectories, due to separatrix crossing. However, separatrix-crossing theory [8] and the theory of phase correlations [9] together constitute a mapping, which we call the separatrix-crossing map, that gives the change in J and its conjugate angle Θ due to a wave-particle interaction. Numerical simulations show that the separatrix-crossing map accurately describes resonant particle dynamics in the limit of small ε.

We have also developed a simple scenario which qualitatively describes the evolution of an arbitrary initial ensemble of test-particles in a periodic array of broad, large-amplitude wave packets and which quantitatively describes the resulting steady-state distribution. The ensemble evolves dramatically during the first few wave-particle interactions as resonant particles strongly scatter with each interaction. On a longer time scale, the ensemble slowly spreads, because the separatrix crossing map is stochastic. In steady state, the distribution is uniformly distributed in momentum throughout separatrix-swept phase space.

The Hamiltonian system studied here provides a crude model for electron dynamics in a strongly turbulent plasma which is characterized by large-scale, narrow-spectrum wave structures. As was noted in Sec. I, a comparison of the numerical work of Graham and Fejer with that of FKRB shows that a coherent wave model yields qualitatively the same dynamics as does an incoherent model, when in the strong turbulence limit. Although it may be impractical to derive a diffusion coefficient for such a system, the stochasticity of the separatrix-crossing map allows one to predict the final distribution function for resonant electrons (given the parameters of the turbulent wave structures), so that one could predict the amount of wave energy that would be lost to resonant particles. Thus our work provides a starting point for a detailed, self-consistent model of strong electrostatic plasma turbulence.

Our Hamiltonian system is also a simple model for electron dynamics in a tokamak with very strong current drive. FKRB had this application in mind. A more explicit example is the microwave tokamak experiment at Lawrence Livermore National Laboratory [26], in which it was proposed that a high power radio-frequency free-electron laser be used to a drive a localized large-amplitude wave in the Alcator-C tokamak. Through application of our methods to the appropriate Hamiltonian, one could deduce the steady state of such a system, which would allow one to calculate the generated current as a function of system parameters.

Finally, our wave packet potential resembles the ponderomotive potential of a Compton regime free-electron laser (FEL) (see, e.g., Eqs. (43) and (60) for Ref. [27]), in the limit that the spatial variations in the wiggler magnet occur over scale lengths long compared to the synchrotron oscillation length of the trapped electrons. The authors discussed in paper I how adiabatic tapering of the magnetic field strength at the wiggler entrance and exit would minimize longitudinal emittance growth (i.e., heating) of the electron beam. This is important in an electron ring FEL for two reasons: first, excessive heating of the electron beam will diminish the resonant coupling between the bunches and the ponderomotive potential during subsequent passes, and second, strong perturbation of the electron beam by the wiggler might disrupt the ring performance. In addition, preliminary analysis [28] has shown that adiabatic trapping into the ponderomotive potential can lead to enhanced energy extraction in a single pass and improved efficiency during multiple passes. Given an appropriately tapered wiggler in a recirculating system, the sort of analysis presented here would allow one to calculate the steady-state longitudinal distribution of the electron beam, which in turn is required for understanding of the steady-state operation of the FEL.

ACKNOWLEDGMENT

This work was supported by the U.S. Department of Energy under Contract No. DE-FG02-86ER40302, and by Grumman Corporation.

APPENDIX

The crossing parameter for each phase space region is defined in Ref. [8] just as we have defined them above in Eqs. (14). Such a definition, however, requires that one numerically integrate the separatrix-crossing trajectory in question, in order to find the value of the Hamiltonian at the critical vertex, $E_{\phi 0}$, if one wishes to know how the adiabatic invariant changes. Once the initial crossing parameter is known, one can then use the theory of phase correlations [9] to obtain subsequent crossing parameters. In order to have a complete separatrix-crossing map which does not depend in any way upon numerical integration of differential equations, here we present an analytic method for determining the initial crossing parameter for arbitrary initial conditions.

We now follow Sec. IV of Ref. [9] by defining q_{-N} as the "time" when a particular trajectory reaches the vertex that is N steps before the critical vertex. We define a *step* to be the portion of a trajectory between two successive vertices. Furthermore, we choose q_{-N} to lie in the interval where both the near-separatrix perturbation theory and adiabatic theory are valid for this trajectory. While the trajectory in question was taken to be in region c for Ref. [9], we consider it to be in one of the other two regions, which we denote by β. Adiabatic theory still holds at the time q_{-N}, so we know that $\Theta_{-N}=0$ (because the trajectory is at a vertex), and that the adiabatic invariant series is given by its initial value $J^1(E_{\phi-N},q_{-N})=J_i$.

The object of this appendix is to take an arbitrary initial condition in region β that will eventually result in a separatrix crossing, and determine analytically the appropriate crossing parameter. We write the coordinates of the initial condition as (J_i,Θ_i,q). Because adiabatic

invariance theory holds for q between q_i and q_{-N}, we know that

$$\Theta_{-N}=\left[\Theta_i+\int_{q_i}^{q_{-N}} dq\, \nu_\beta^1(J_i,\lambda\equiv\varepsilon q)\right]_{\text{mod }1}=0\ , \tag{A1}$$

which means that the quantity in the brackets must be some integer n. This equation is analogous to Eq. (27) of Ref. [9].

We can rewrite the integral on the right-hand side of Eq. (A1) in the form

$$\int_{q_i}^{q_{-N}} dq\, \nu_\beta^1(J_i,\lambda)=\Phi_{i\beta}(J_i,q_i)-\int_{q_{-N}}^{q_x} dq\, \nu_\beta^1(J_i,\lambda)\ , \tag{A2}$$

which is analogous to Eq. (29) of Ref. [9]. We call $\Phi_{i\beta}$ the initial phase advance function for region β, in order to distinguish it from the phase advance function Φ_β, which is defined in Eq. (18c) above and in Eq. (38) of Ref. [9]. The initial phase function is defined by

$$\Phi_{i\beta}(J_i,q_i)\equiv\varepsilon^{-1}\int_{\lambda_i}^{\lambda_x} d\lambda\, \nu_\beta^1(J_i,\lambda)\ . \tag{A3}$$

The integral on the right-hand side of Eq. (A2) has essentially been evaluated in Ref. [9]. Following Ref. [9], we change the variable of integration from the time q to the value of the first-order corrected Hamiltonian. The result, to lowest order in ε, is

$$\int_{q_{-N}}^{q_x} dq\, \nu_\beta^1(J_i,\lambda)=\frac{K_\beta^1(J_i,\lambda_x)-K_\beta^1(J_i,\lambda_{-N})}{\dot{Y}_\beta(\lambda_x)}\ , \tag{A4}$$

which is analogous to Eq. (32b) of Ref. [9]. If we now use Eqs. (20a) and (35) from Ref. [9], as well as the definition of the crossing parameter, we obtain the following lowest-order result:

$$\int_{q_{-N}}^{q_x} dq\, \nu_\beta^1(J_i,\lambda)=M_\beta+N\ . \tag{A5}$$

At this point, we can use Eqs. (A1), (A2), and (A5) to obtain the result

$$M_\beta=\text{frac}[\Theta_i+\Phi_{i\beta}(J_i,q_i)]\ , \tag{A6}$$

where $\Phi_{i\beta}$ must be obtained, in general, via quadrature.

[1] L. Landau, J. Phys. (U.S.S.R.) **10**, 25 (1946); J. Dawson, Phys. Fluids **4**, 869 (1961).

[2] A. A. Vedenov, E. P. Velikhov, and R. Z. Sagdeev, Usp. Fiz. Nauk **73**, 701 (1961) [Sov. Phys. Usp. **4**, 332 (1961)]; W. E. Drummond and D. Pines, Ann. Phys. **28**, 478 (1964).

[3] T. H. Dupree, Phys. Fluids **9**, 1773 (1966).

[4] F. Doveil and D. Grésillon, Phys. Fluids **25**, 1396 (1982).

[5] V. Fuchs, V. Krapchev, A. Ram, and A. Bers, Physica D **14**, 141 (1985).

[6] K. N. Graham and J. A. Fejer, Phys. Fluids **19**, 1054 (1976).

[7] M. Kruskal, J. Math. Phys. **3**, 806 (1962).

[8] J. R. Cary, D. F. Escande, and J. L. Tennyson, Phys. Rev. A **34**, 4256 (1986).

[9] J. R. Cary and R. T. Skodje, Physica D **36**, 287 (1989).

[10] A. V. Timofeev, Zh. Eksp. Teor. Fiz. **75**, 1303 (1978) [Sov. Phys. JETP **48**, 656 (1978)].

[11] A. I. Neishtadt, Fiz. Plazmy **12**, 992 (1986) [Sov. J. Plasma Phys. **12**, 568 (1986)]; Fiz. Plazmy **13**, 765(E) (1987) [Sov. J. Plasma Phys. **13**, 441 (1987)].

[12] D. L. Bruhwiler and J. R. Cary, Phys. Rev. Lett. **68**, 255 (1992).

[13] D. L. Bruhwiler and J. R. Cary, Part. Accel. **43**, 195 (1994).

[14] D. F. Escande, in *Plasma Theory and Nonlinear and Turbulent Processes in Physics,* edited by V. G. Baryakhtar, V. M. Chernousenko, N. S. Erokhin, A. G. Sitenko, and V. E. Zakharov (World Scientific, Singapore, 1988), p. 398.

[15] D. L. Bruhwiler and J. R. Cary, Physica D **40**, 265 (1989).

[16] C. R. Menyuk, Phys. Rev. A **31**, 3282 (1985).

[17] Y. Elskens and D. F. Escande, Nonlinearity **4**, 615 (1991).

[18] T. J. Kaper and S. Wiggins, Physica D **51**, 205 (1991).

[19] V. I. Arnol'd and A. Avez, *Ergodic Problems of Classical Mechanics* (Addison-Wesley, Redwood City, CA 1989), pp. 16 and 17; A. J. Lichtenberg and M. A. Lieberman, *Regular and Stochastic Motion* (Springer-Verlag, New York, 1983), pp. 260 and 261.

[20] R. M. Kulsrud, Phys. Rev. **106**, 205 (1957); A. Lenard, Ann. Phys. **6**, 261 (1959).

[21] R. W. B. Best, Physica **40**, 182 (1968).

[22] C. Gardner, Phys. Rev. **115**, 791 (1959); R. G. Littlejohn, J. Plasma Phys. **29**, 111 (1983).

[23] R. T. Skodje and J. R. Cary, Comp. Phys. Rep. **8**, 221 (1988).

[24] I. S. Gradshteyn and I. M. Ryzhik, *Table of Integrals, Series and Products* (Academic, New York, 1980).

[25] D. L. Bruhwiler, Ph.D. thesis, University of Colorado, Boulder, 1990.

[26] W. M. Nevins, T. D. Rognlien, and B. I. Cohen, Phys. Rev. Lett. **59**, 60 (1987).

[27] C. W. Roberson and P. Sprangle, Phys. Fluids B **1**, 3 (1989).

[28] S. Hendrickson, J. R. Cary, S. Robertson, and S. Makoski, Bull. Am. Phys. Soc. **37**, 1456 (1992); S. Hendrickson, J. R. Cary, and S. Robertson, *ibid.* **38**, 1328 (1993).

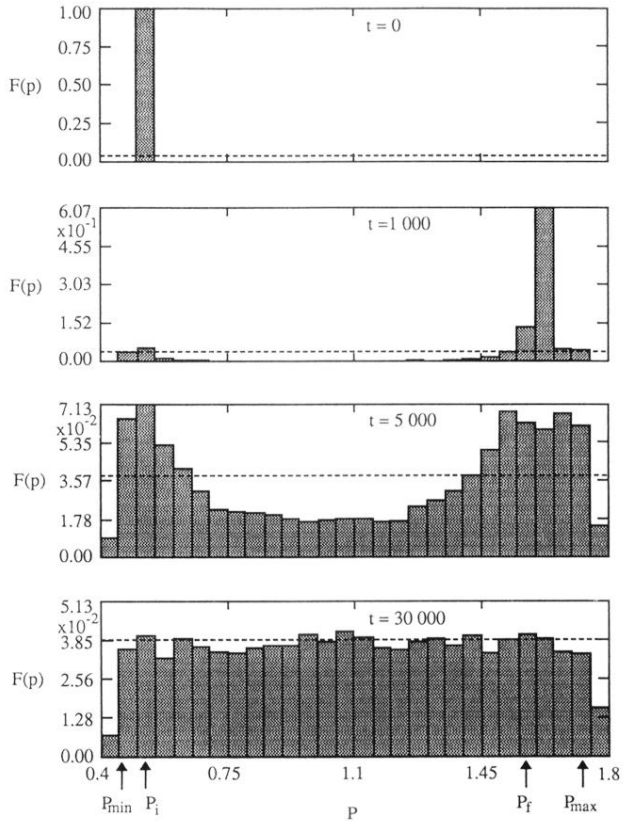

FIG. 5. Time evolution of the momentum distribution function $F(p)$ for 5×10^3 test particles interacting with the wave packet shown in Fig. 4.